

Electromagnetic and Mechanical Stress Analysis of Wind-Driven Synchronous Reluctance Generator

Kitaba Tefera, Praveen Tripathy *Senior, Member IEEE*, and Ravindranath Adda, *Senior Member, IEEE*.

Abstract—The investigation explores the mechanical stress and electromagnetic performance for a wind-driven synchronous reluctance generator (SRG). The change in the mechanical stress due to the presence of centripetal force, wind speed, and rotor speed are evaluated for different thickness of tangential and radial ribs. Moreover, the variation in the electromagnetic feature such as the q - and d -axes flux, reactance ratio, inductance, torque and torque ripple are discussed for different thickness of tangential and radial ribs. Increasing both tangential and radial ribs thickness has an effect on the electromagnetic performance, but it is observed that effect is significantly more with the variation of tangential rib thickness. Similarly, the mechanical stress analysis for rotor design has been explored in this paper. It is observed that high concentration of peak stress on the rotor ribs, which limits the range of rotor speed.

Index Terms—Electromagnetic, mechanical integrity, synchronous reluctance generator, stress and safety factor, wind speed.

NOMENCLATURE

R_t	Wind turbine radius.
Ω	Blade tip speed.
\mathfrak{R}_d	d -axis reluctance.
\mathfrak{R}_q	q -axis reluctance.
L_{ls}	Stator leakage inductance.
Ω	Rotor rated speed.
ξ	Saliency ratio.
Gr	Gear ratio.
l	Tip speed ratio.
J	Current density.
D_o	Stator air gap diameter.
D_{in}	Stator yoke diameter.
D_r	Rotor outer diameter.
R_s	Phase resistance.
E_{ph}	Phase induced.
I_d	d -axis current.
I_q	q -axis current.
X_d	d -axis reactance.
X_q	q -axis reactance.
P	Number of poles.
m	Number of conductor turns per phase.
I_{ph}	RMS phase current.
l_g	Air gap length.

M_a	Flux line lamination mass.
L	Stack length.
P_{rated}	Machine rated power.
T_{rated}	Machine rated torque.
λ_q	q -axis flux.
λ_d	d -axis flux.
L_q	q -axis inductance.
L_d	d -axis inductance.
SF	Stress intensity factor.
f	Centripetal force.
T_{ave}	Average torque.
T_{rip}	Torque ripple.

I. INTRODUCTION

THE mechanical stress analysis and electromagnetic performance of wind-driven rotor of synchronous reluctance generator (SRG), plays an important role towards validating the rotor design. The topology associated with the design of SRG rotors are either transversely laminated variant (TLV) or axially laminated variant (ALV) [1] types, but the TLV design is more commonly used over ALV [2]. Hence, the paper investigates the rotor of the TLV type. Significant literature is available in the design of flux barriers number and their shape insulation ratio [3], [4]. Park et al. [5], Mohammadi et al. [6] and Di Nardo et al. [7] has investigated different computational and analytical barriers optimization methods.

Similarly, significant work has been done towards the selection of material grade used in wind-driven of SRG design [8]–[10]. But, a very few and rare studies have been carried out on the analysis and design of mechanical stress and electromagnetic performance with respect to radial and tangential ribs that links the flux lines. This paper full fill the literature gap in this area.

An SRG design base on a high power factor and high reactance ratio i.e., high X_d/X_q for better performance is achieved through the high-quality design of rotor. The design evolves the number of barriers, shape, and the number of poles along with the design of tangential and radial ribs to ensure good performances. The SRG coupled with the wind turbine experiences a wide variation of centripetal or centrifugal force acting on the rotor, and hence, requires the electromagnetic and mechanical stress analysis of the SRG. For low wind speed centripetal load is less, but to have better electromagnetic performance, the design of rotor should be such that the q -axis inductance reduces and the d -axis inductance increase [1], but this is achieved by a decrease in the thickness of radial and tangential ribs. The design based on the reduced thickness of

Manuscript was submitted for review on 25, January, 2019.

This work was sponsored by a Defense University from the National Defense of Ethiopia.

K. Tefera, P. Tripathy and R. Adda are with the Department of Electronics and Electrical Engineering, Indian Institute of Technology, Guwahati, Assam (e-mail: tepera@iitg.ac.in)

Digital Object Identifier 10.30941/CESTEMS.2019.00015

axial and tangential ribs leads towards high stress on the ribs, and hence, is not suitable for high speed. Hence, a trade-off between mechanical and electromagnetic performances with the variation of wind speed is required to validate the design. It is observed from the literature review that the electromagnetic-mechanical analysis of SRG rotor design with the variation of wind speed in self-excited mode is not covered in the available literature. Therefore, this paper focuses on the trade-off between mechanical and electromagnetic performances with the variation of wind speed and thickness of tangential and radial ribs. The finite element analysis (FEA) is used for both mechanical stress analysis and electromagnetic analysis in this paper. The considered SRG have been designed for producing 12.7 Nm of torque at 1500 rpm equal to 2:1 kW with the efficiency of 82%, with stator fill factor of 50%, is shown in Fig. 1. The major contributions of this paper are:

- Electromagnetic-mechanical analysis of wind-driven synchronous reluctance generator using FEA.
- By varying the rotor design parameters such as radial and tangential ribs thickness, how the electromagnetic-mechanical performances vary.

This paper is organized as follows: The second Section present problem statements. The third Section provides the electromagnetic performance and its result analysis. Mechanical performance and its results are discussed in Section 4, and finally, the conclusions are given in Section 5.

II. MACHINE DESIGN PARAMETERS AND PROBLEM STATEMENT

A. Design Specification And Parameters

The geometrical dimension and specifications of the SRG are summarized in Table I. The air gap length is fixed to the range, as allowed by the manufacturer ($l_g = 0.35 \text{ mm}$). It is important to note that as the air gap length increases, the torque and power factor decreases [1], [10]. While designing the machine, it is common to use distributed winding, to reduce harmonic content of the stator EMF, which negatively impacts the reluctance torque and the core losses [11]. The present design has four numbers of poles, and the design can be extended for more number of poles. For a better design, in terms of iron losses, torque ripple, and mechanical strength, typically the number of flux barriers are approximately half of the number of slots per pole. Hence, the present design uses five flux barriers per pole with 36 stator slots as shown in Fig. 1.

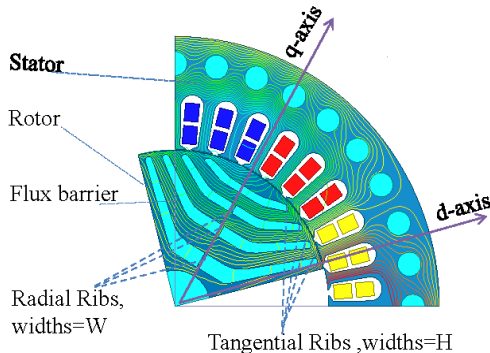


Fig. 1. Structural, cross-section and dq -axes rotor reference frame of SRG.

The detailed sizing and design procedure of the SRG start by assigning the initial key parameters of the wind turbine such as speed, maximum torque, and thermal analysis of the machine, and the designed machine with its parameters is summarized in Table I. The present work, does the mechanical stress analysis of the designed machine, with varying the rotor speed and study its influence on the rotor design of SRG. Here, the stator is assumed to be fixed at all case.

TABLE I
MACHINE SPECIFICATION AND DESIGN PARAMETERS OF 2:1 kW
GENERATOR

Parameters	Values	Parameters	Values
λ	8 rad	Gr	2.2
Rt	1.34 m	Ω	72 rad/s
Lms	89.4 mH	Do	180 mm
Dr	104 mm	mIq	290 A. turns
Din	104.7 mm	P	4
ω_{rated}	1500 rpm	mIa	81 A.turns
Rs	1.176 Ω	Lls	3.57 mH
lg	0.35 mm	Trated	12.7 Nm
Ld	90 mH	Im	14.14 A
Lq	7.15 mH	J	$\leq 9 \text{ A/mm}^2$
Eph	150 V	L	65 mm
lph	10 A	Prated	2.1 km

B. Rotor Parametirizations

In the surveys, different kind of rotor flux barrier parameterizations have been given [12]–[14]. All the findings show that the flux barrier and tangential barrier structure play the main role on torque ripple minimization and torque maximization [15]. Mostly, it is observed that the performances could be improved by using complex design, i.e., increasing the number of bridges etc, but the complex design significantly increases the cost of production, difficult to manufacture, and also involves a high cost for its design [14], [16]. Hence the present work has used only four number of poles, and shown in Fig. 1. Every flux barrier is consists of trapezoid shape segments and identified by the tangential thickness H , radial thickness W and the end point angle at the air gap, α_m that have to assures the structural integrity at high-speed as shown in Fig. 2(b). The expression for maximum rotor tips mechanical end point angle α_m , in terms of number of barriers (k_i), poles pair (p) and floating angle (β) as (1) [17]:

$$\alpha_m = \frac{((\pi/2p) - \beta)}{(k_i - 1/2)} \quad (1)$$

Here, the floating angle β assumed to be in between 0 to 10° . When compared to other generators such as ac generator and IG, the SRG has the following advantages:

- There is no copper winding in the rotor. Thus, the SRG is less in cost and no copper losses in the rotor.
- It reduces the risk of frequency and phase voltage variation in case of load change/ fault.
- It has high torque density and efficiency.

In spite of these advantages, care must be taken while designing rotor of SRG for high wind speed application, to insure that the machine is mechanically stable, and produces more electromagnetic torque with minimal ripples

III. ANALYSIS OF ELECTROMAGNETIC PERFORMANCE

The electromagnetic performance of SRG rotor improves by minimizing the reluctance of the d -axis, $\mathfrak{R}d$ and maximizing the reluctance of the q - axis, $\mathfrak{R}q$. The ratio of d - axis inductance to the q -axis inductance (saliency ratio) is usually defined using the orthogonal axis inductances, $L_d \propto 1/\mathfrak{R}d$ and $L_q \propto 1/\mathfrak{R}q$ [13]. This inductance ratio is denoted as ξ , as given below

$$\left\{ \begin{array}{l} \xi = \frac{L_d}{L_q} \\ \text{or} \\ \xi = \frac{X_d}{X_q} \end{array} \right. \quad (2)$$

For better electromagnetic performance, this ratio needs to be large. It is observed that by reducing the thickness of ribs (i.e., for both radial and tangential ribs), as shown in Figs. 4, 5, the inductance ratio (ξ) tends to increase, but mechanical stress tends to increase, hence, a design choice need to be made between these conflicting objectives. Fig. 2(a) and 2(b) shows the variation of d and q -axes inductances with respect to the change of q and d -axes currents. This plot is associated with the rotor cross-section, with the radial rib thickness ($W = 1 \text{ mm}$) and tangential ribs thickness ($H = 1.2 \text{ mm}$), respectively. The curves obtained from curve fit, and FEA can be distinguished by the smoothed and dotted lines as presented in Fig. 2(a). The L_d of the SRG keeps increasing for low values of current. However, as the current becomes approximately more than 5 A , the value of L_d starts decreasing and attains a constant value because of the magnetic saturation.

While the L_q of SRG is high for the low value of current due to the presence of bridge in q -axis, it decreases gradually with the increase of current and subsequently becomes constant. The important point to note that in the designed SRG, the thickness of tangential and radial ribs (See Fig 3) plays an important role in controlling the q - and d -axis fluxes, hence, control the associated inductances. Fig. 4, shows the effect of variation in tangential rib thickness on d - q axis fluxes, the ratio of d and q axis inductances and reactants while keeping the thickness of radial ribs to a value of $W_{max} = 1 \text{ mm}$. From Fig. 4(a), it is observed that as the thickness of tangential rib is reduced, the value of λ_d increases, whereas, the value of λ_q decrease till the ratio of (X_d/X_q) is maximum, as given in Fig. 4(b). Similarly, the plot of d and q axis inductances is shown in Fig. 4(c). It is also observed that as the core start getting saturated, there is a decrease in (X_d/X_q) ratio. Fig. 5, shows the effect of variation in radial rib thickness on d - q axis fluxes, the ratio of d and q axis inductances and reactants while keeping the thickness of tangential ribs to a value of $H_{max} = 1.2 \text{ mm}$. From Fig. 5(a), it is observed that as the thickness of radial rib is reduced, the value of λ_d slightly increases, whereas, the value of λ_q decrease till the ratio of (X_d/X_q) is maximum, as given in Fig. 5(b). Similarly, the plot of d and q axis inductances is shown in Fig. 5(c). It is also observed from Figs. 4, 5, that the effect of

variation on inductance is more with the change in thickness of tangential ribs, as compared with the variation in thickness of radial ribs.

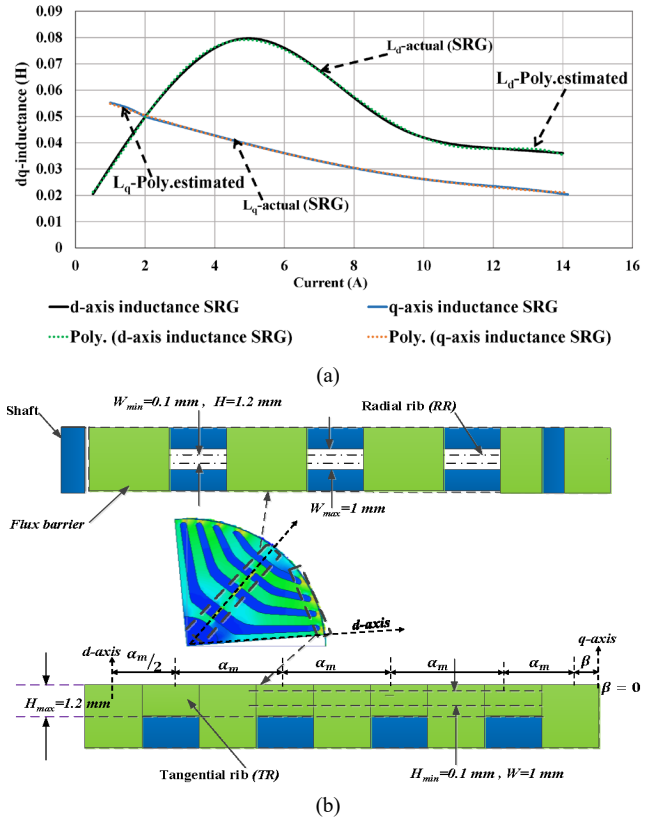


Fig. 2. (a) d and q -axes magnetizing characteristic of SRG. (b) Rotor cross section view: radial and tangential ribs thickness.

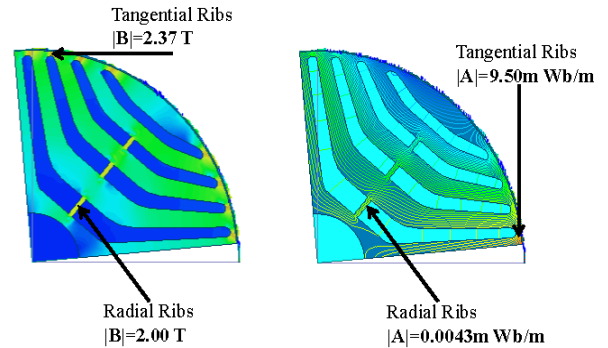
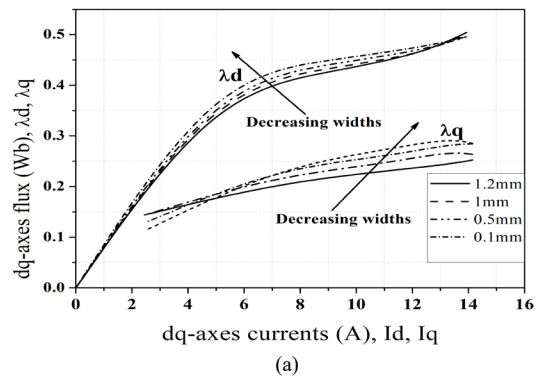


Fig. 3. Magnetic field density and flux lines plot showing ribs saturation.



(a)

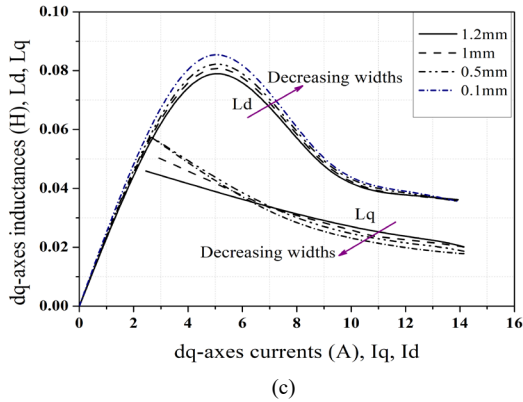
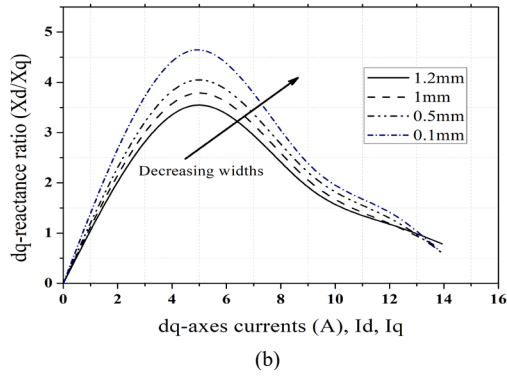


Fig. 4. (a) d - and q -axes flux linkages magnetizing curve with tangential rib widths. (b) d - and q -reactance ratio with tangential rib widths. (c) d - and q -inductances with tangential rib widths.

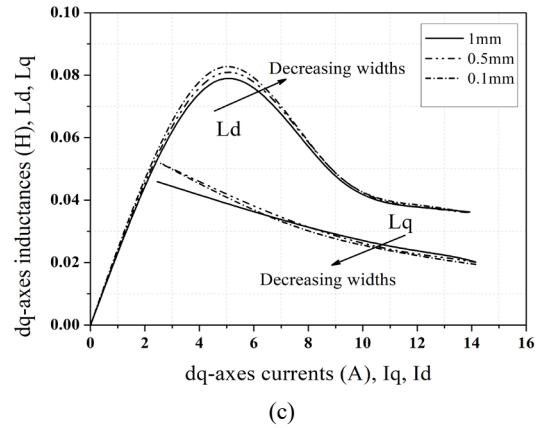
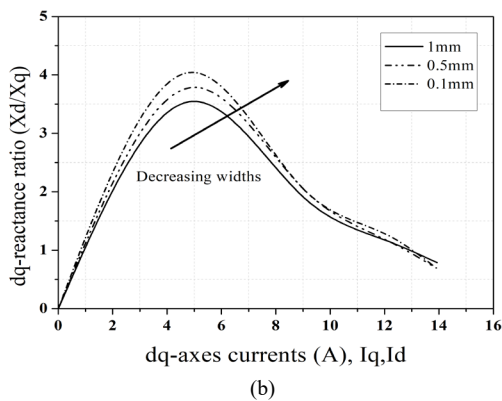
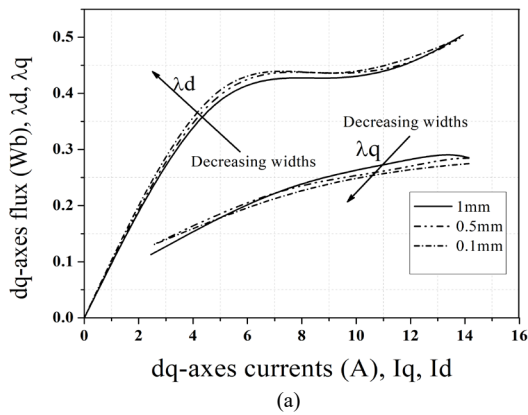


Fig. 5. (a) d - and q -axes flux linkages magnetizing curve with radial rib widths. (b) d - and q -reactance ratio with radial rib widths. (c) d - and q -inductances with radial rib widths.

In summary, the tangential and radial ribs should be small enough to produce good electromagnetic performance, i.e., to reduce the q -axis inductance and maximize the d -axis inductance (increasing reluctance torque), but the mechanical stress in the ribs should be below the centripetal loading. Fig. 6(a) shows that the performance of machines in motoring and generating mode. Fig. 6(a), the effect of reducing tangential rib i.e., with rib thickness 1:2 mm, 1 mm, 0:5 mm and 0:1 mm is shown while keeping the thickness of radial ribs to a value of $W_{max} = 1$ mm. It is observed that as the thickness of tangential rib reduces, the torque increase in motoring or generating modes, as shown in Fig. 6(a), mainly because the magnetic flux flowing outward from the rotor q -axis reduces, hence, reducing the value of L_q . Similarly, in Fig. 6(b), the effect of reducing radial rib width i.e., with rib thickness 1:2 mm, 1 mm, 0:5 mm and 0:1 mm is shown while keeping the thickness of tangential ribs to a value of $H_{max} = 1:2$ mm.

It is observed that as the thickness of the radial rib reduces, the torque slightly increase in motoring or generating modes, as shown in Fig. 6(b), mainly due to the reduction of magnetic flux in q -axis. However, it is observed that the effect of radial ribs width variations on torque is not much as compared with the variation of tangential rib widths. From Fig. 6(a) and Fig. 6(b), it is observed that the average torque is as a function of square of stator current till the current of the machine is 5A. However, after 5A the difference between $(L_d - L_q)$ is approximately constant as seen from Fig. 2(a), hence, the variation of average torque is observed to be linear. The influences of the tangential rib width on torque ripple while keeping the thickness of radial ribs to a value of $W_{max} = 1$ mm are shown in Fig. 7(a). From Fig. 7(a) it can be observed that the torque ripple increases by reducing the tangential rib thickness. Similarly, the effect on torque ripple for the variation of radial rib thickness while keeping the thickness of tangential ribs to a value of $H_{max} = 1:2$ mm is shown in Fig. 7(b). It is observed, that the torque ripple decrease by reducing the radial rib thickness. When the radial rib width is reduced, both the magnetic and air reluctance layers increase for q -axis flux, that causes L_q to reduce, while L_d almost remains constant.

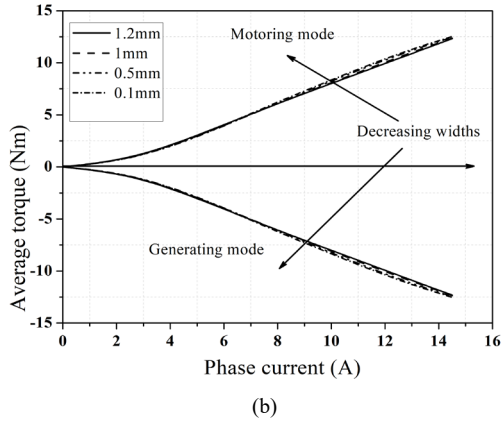
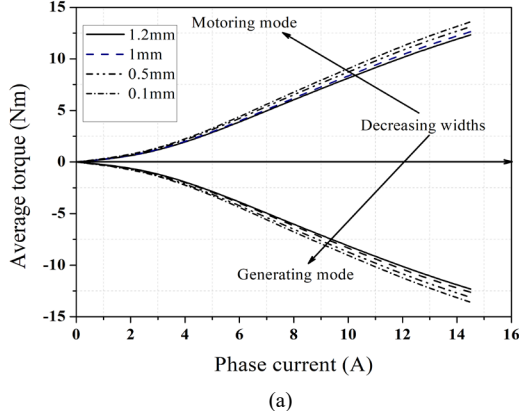


Fig. 6. (a) Average torque-current profile of SRG curve with tangential rib widths. (b) Average torque-current profile of SRG curve with radial rib widths.

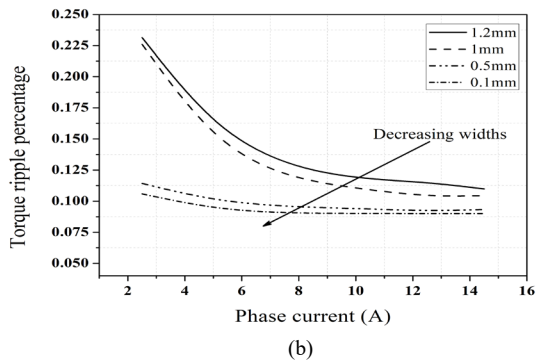
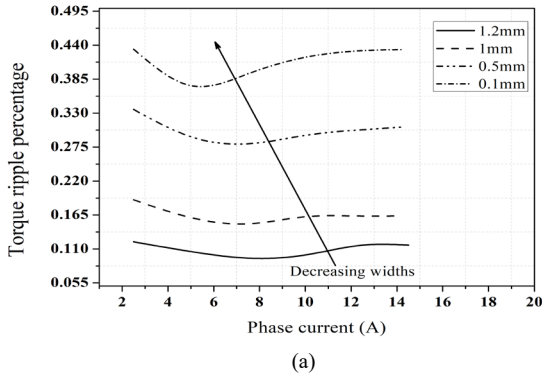


Fig. 7. (a) Torque ripple percentage curve with tangential rib widths. (b) Torque ripple percentage curve with radial rib widths

IV. ANALYSIS OF MECHANICAL PERFORMANCE

From the analysis of electromagnetic performance, as discussed in the previous section, we observed that for better electromagnetic performance, the thickness of ribs need to be reduced, but as these ribs also provide mechanical strength to the rotor, it is important to know the stress in these ribs, under the influence of centripetal force, and check whether the stress is within the permissible limit.

A. Centripetal Force of Flux Barriers

It can be seen from Fig. 1, that mainly the radial ribs, support the flux barriers together under influence of centripetal force while operating at variable speed. The flux guides lamination has a mass of [10]:

$$M_a = \rho L \iint dA \quad (3)$$

Where, L is the stack length, $\iint dA$ is the cross-section area of the flux barriers, which has a complex shape, and ρ is the density of lamination material. When the generator is operating with the rotational speed of ω , the centripetal force acting towards the centre of the rotor (i.e., normally) with radius R at the surface of the rotor is given as:

$$f = M_a R \omega^2 \quad (4)$$

The yield strength δ_y , is the stress above which the material become plastic, and hence, the stress on a rotor must be below the yield strength of the material used in the design of rotor. From, equation (4), it can be observed that the stress on the rotor is a function of ω^2 . Usually, the stress must be less than yield strength with an acceptable safety factor while designing and/or sizing the tangential and radial ribs.

The lamination material (50C350-AP) is used in the design of the rotor for SRG, which has average yield strength is 310 *Mpa*, and the lamination density of 7874 *kg/m³*. The commonly used safety factor S_f is given as per the equation below:

$$S_f = \delta_y / \sigma_p \quad (5)$$

Where, δ_y is the average yield strength of the material, σ_p is the stress on the rotor. Fig. 8 shows the distribution of mechanical stress at different parts of SRG rotating at 1500 *rpm* using finite element analysis (FEA). The peak stress observed at the critical points of the rotor are reported as in Fig.8, and can be observed that the ribs are highly stressed. To provide the quantitative analysis, Table II, and III provides the details about peak stress observed in ribs i.e., in tangential ribs indexed as 1,2,3 and 4 i.e., $TR_{1,2,3,4}$ and radial ribs index as 1,2, and 3 i.e., $RR_{1,2,3}$. The results shown in Table II corresponds to the rotor rotating at 1500 *rpm*, with the simultaneous variation in thickness of both tangential ribs (TR) and radial ribs (RR) by same thickness i.e., the thickness of both (TR/RR) are same and varies from 1,2 *mm* to 0.1 *mm*. The table also provides a stress factor (SF), centripetal force at the surface of the rotor (f), average torque (T_{av}), and percentage torque ripple (T_{rip}). Similarly, Table III provides the similar analysis for rotor rotating at 2500 *rpm*, i.e., 60% over the rated speed of 1500 *rpm*.

TABLE II

MECHANICAL PERFORMANCE (VON MISES STRESS, CENTRIPETAL FORCE, STRESS FACTOR) OF PEAK STRESS AND ELECTROMAGNETIC PERFORMANCE (TORQUE AND RIPPLE) OF THE DESIGNED ROTOR SPEED OF 1500 RPM

Thickness	(TR/RR) → 1.2 mm	1 mm	
Parameters	Peak stress	Peak Stress	Unit
$TR_{1,2,3,4}$	38	57	Mpa
$RR_{1,2,3}$	23	34	Mpa
SF	1515	1406	Mpa
f	908	902	N
T_{av}	12.28	12.63	Nm
$T_{rip}(\%)$	11	16	-

Thickness	(TR/RR) → 0.5 mm	0.1 mm	
Parameters	Peak stress	Peak Stress	Unit
$TR_{1,2,3,4}$	72	172	Mpa
$RR_{1,2,3}$	65	245	Mpa
SF	1253	313	Mpa
f	980	880	N
T_{av}	13.41	14.08	Nm
$T_{rip}(\%)$	26	36	-

TABLE III

MECHANICAL PERFORMANCE (VON MISES STRESS, CENTRIPETAL FORCE, STRESS FACTOR) OF PEAK STRESS AND ELECTROMAGNETIC PERFORMANCE (TORQUE AND RIPPLE) OF THE DESIGNED ROTOR SPEED OF 2500 RPM

Thickness	(TR/RR) → 1.2 mm	1 mm	
Parameters	Peak stress	Peak Stress	Unit
$TR_{1,2,3,4}$	98	146	Mpa
$RR_{1,2,3}$	69	88	Mpa
SF	1137	888	Mpa
f	2323	2310	N
T_{av}	12.23	12.50	Nm
$T_{rip}(\%)$	9	13	-

Thickness	(TR/RR) → 0.5 mm	0.1 mm	
Parameters	Peak stress	Peak Stress	Unit
$TR_{1,2,3,4}$	184	440	Mpa
$RR_{1,2,3}$	168	565	Mpa
SF	496	1719	Mpa
f	2277	2270	N
T_{av}	13.40	14.05	Nm
$T_{rip}(\%)$	27	37	-

B. TANGENTIAL AND RADIAL RIB THICKNESS

This section analysis the effect on stresses estimated for SRG with simultaneous variation in thickness of both tangential ribs (TR) and radial ribs (RR) by same thickness. For the estimation of stress, the present work uses finite element analysis (FEA). From Fig. 8, it could be observed that ribs i.e., tangential or radial are the one which is associated with high stress as compared with other parts of the rotor. Hence, this section analysis the stress at tangential and radial ribs in details. Fig. 9(a), show the stress experienced by the tangential rib of different widths with the variation of centripetal force.

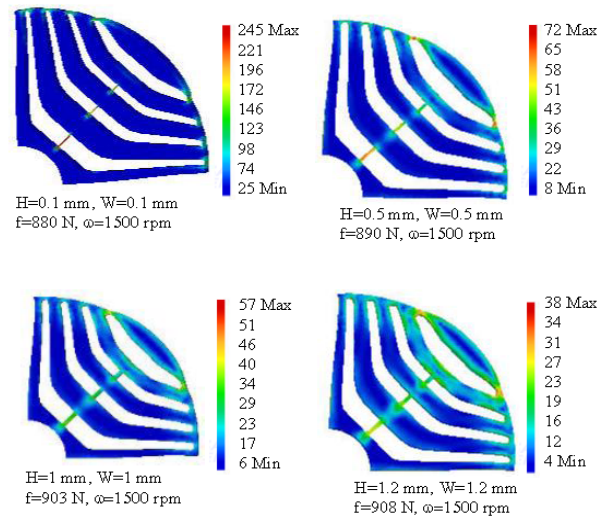
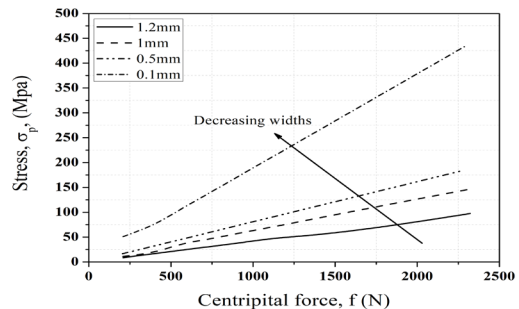


Fig. 8. Von Mises stress distributions (Mpa) of designed rotor with ribs widths variation (minimum=0.1 mm to maximum=1.2 mm)

Similarly, Fig. 9(b), shows that the stress observed at the radial rib. From the results, it can be observed that the stress reduced with increasing ribs width. It is also observed that the variation of stress with an increase in centripetal force is approximately linear. Fig. 10 (a) provides the plot associated with the stress in tangential ribs of thickness varying from 0:1 mm to 1:2 mm. It is observed that as the ribs thickness decrease, the stress in tangential rib increase, and increases with the increase of rotor speed. It is also observed that the increase in stress on tangential ribs is approximately quadric to the variation of rotor speed. Fig. 10(b), provides a plot of safety factor in the tangential rib with different widths vs rotor speed. The zoomed version of the plot shows the yield strength line corresponding to the safety factor of 1, but it is common to take a safety factor of 2:5 for most of the design, hence, the present work also use a safety factor of 2:5, as shown by a dashed line in the plot. It can also be observed that a thickness of 1:2 mm or more is required to provide mechanical stability of the tangential rib. Similarly, Fig. 11 (a) provides the plot associated with the stress in radial ribs of thickness varying from 0:1 mm to 1:2 mm. It is observed that as the ribs thickness decrease, the stress in radial rib increase, and increases with the increase of rotor speed.

It is also observed that the increase in stress on radial ribs is approximately quadric to the variation of rotor speed. Fig. 11(b), provides a plot of safety factor in the radial rib with different widths vs rotor speed. It can also be observed that a thickness of radial rib should be more or equal to 1:0 mm for ensuring mechanical stability of the ribs.



(a)

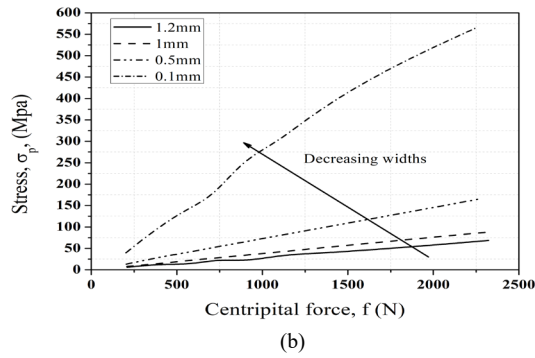


Fig. 9. (a) Stress at tangential rib with different widths vs Centripetal force. (b) Stress at radial rib with different widths vs centripetal force.

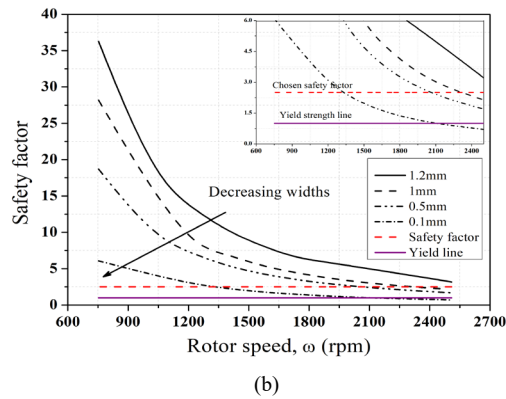
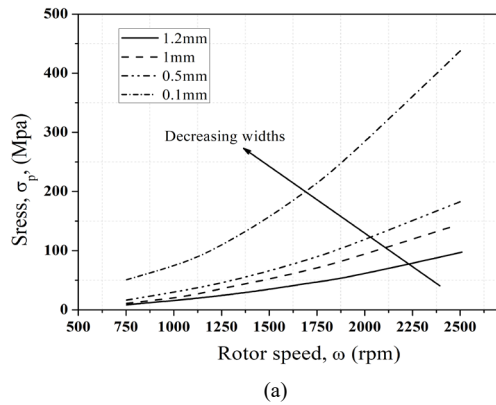


Fig. 10. (a) Stress at tangential rib with different widths vs rotor speed. (b) Safety factor of tangential rib with different widths vs rotor speed.

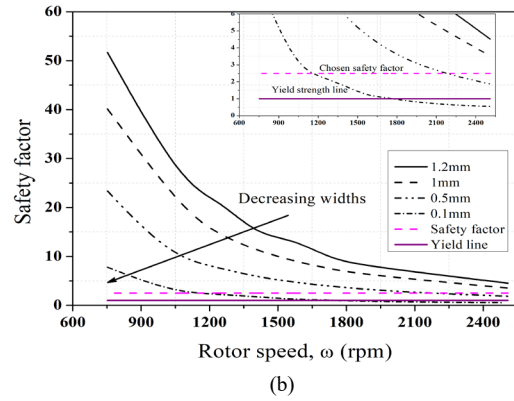
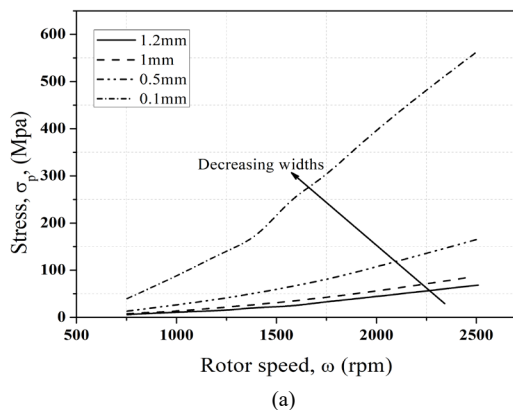


Fig. 11. (a) Stress at radial rib with different widths vs rotor speed. (b) Safety factor of radial rib with different widths vs rotor speed.

V. CONCLUSION

The present paper has presented the mechanical stress and electromagnetic analysis of SRG for a rotor with transverse lamination. The first part of the paper mainly discuss how the thickness of ribs affect the electromagnetic performances of the machine i.e., it is observed that with decrease in the thickness of both radial or tangential ribs, there is an increase in the inductance ratio, which reaches to its peak value near to its rated current, and then there is a decrease in this ratio due to the effect of saturation in the core. Further, the mechanical stress analysis is done to find the minimum thickness of the ribs which could ensure mechanical stability. It is also observed that the maximum stress is either at tangential ribs or radial rib of the SRG rotor. To ensure the mechanical stability, a safety factor of 2:5 is used in the present work while suggesting the minimum thickness of the ribs.

REFERENCES

- [1] C. M. Donaghy-Spargo, "Electromagnetic-mechanical design of synchronous reluctance rotors with fine features," *IEEE Transactions on Magnetics*, vol. 53, no. 11, pp. 1–8, 2017.
- [2] T. Matsuo and T. A. Lipo, "Rotor design optimization of synchronous reluctance machine," *IEEE Transactions on Energy Conversion*, vol. 9, no. 2, pp. 359–365, 1994.
- [3] E. Obe, "Calculation of inductances and torque of an axially laminated synchronous reluctance motor," *IET electric power applications*, vol. 4, no. 9, pp. 783–792, 2010.
- [4] R.-R. Moghaddam and F. Gyllensten, "Novel high-performance synrm design method: An easy approach for a complicated rotor topology," *IEEE Transactions on Industrial Electronics*, vol. 61, no. 9, pp. 5058–5065, 2014.
- [5] J. M. Park, S. I. Kim, J. P. Hong, and J. H. Lee, "Rotor design on torque ripple reduction for a synchronous reluctance motor with concentrated winding using response surface methodology," *IEEE Transactions on Magnetics*, vol. 42, no. 10, pp. 3479–3481, 2006.
- [6] M. Mohammad, T. Rahman, R. Silva, M. Li, and D. Lowther, "A computationally efficient algorithm for rotor design optimization of synchronous reluctance machines," *IEEE Transactions on Magnetics*, vol. 52, no. 3, pp. 1–4, 2016.E
- [7] M. Di Nardo, G. L. Calzo, M. Galea, and C. Gerada, "Design optimization of a high speed synchronous reluctance machine," *IEEE Transactions on Industry Applications*, vol. 54, no. 1, pp. 233–243, 2018.
- [8] M. Ibrahim, P. Sergeant, and E. M. Rashad, "Synchronous reluctance motor performance based on different electrical steel grades," *IEEE Transactions on Magnetics*, vol. 51, no. 11, pp. 1–4, 2015.

- [9] S. Taghavi and P. Pillay, "A novel grain-oriented lamination rotor core assembly for a synchronous reluctance traction motor with a reduced torque ripple algorithm," *IEEE Transactions on Industry Applications*, vol. 52, no. 5, pp. 3729–3738, 2016.
- [10] C. M. Spargo, B. C. Mecrow, J. D. Widmer, C. Morton, and N. J. Baker, "Design and validation of a synchronous reluctance motor with single tooth windings," *IEEE transactions on energy conversion*, vol. 30, no. 2, pp. 795–805, 2015.
- [11] C. M. Spargo, B. C. Mecrow, and J. D. Widmer, "A semi numerical finite element post processing torque ripple analysis technique for synchronous electric machines utilizing the air-gap Maxwell stress tensor," *Magnetics, IEEE Transactions on*, vol. 50, no. 5, pp. 1–9, 2014.
- [12] D. Staton, T. Miller, and S. Wood, "Maximising the saliency ratio of the synchronous reluctance motor," in *IEE Proceedings B-Electric Power Applications*, vol. 140, no. 4, IET, pp. 249–259, 1993.
- [13] I. Boldea, "Reluctance synchronous machines and drives (monographs in electrical and electronic engineering)," 2002.
- [14] A. Saleem, N. Alatawneh, R. R. Chromik, and D. A. Lowther, "Effect of shear cutting on microstructure and magnetic properties of non-oriented electrical steel," *IEEE Transactions on Magnetics*, vol. 52, no. 5, pp. 1–4, 2016.
- [15] R. I. Stephens, A. Fatemi, R. R. Stephens, and H. O. Fuchs, *Metal fatigue in engineering*. John Wiley & Sons, 2000.
- [16] J. Ikaheimo, J. Kolehmainen, T. Kansakangas, V. Kivela, and R. R. Moghaddam, "Synchronous high-speed reluctance machine with novel rotor construction," *IEEE Transactions on Industrial Electronics*, vol. 61, no. 6, pp. 2969–2975, 2014.
- [17] M. R., *Synchronous reluctance machine (SynRM) design*. KTH Royal Institute of Technology, 2007.
- [18] C.-T. Liu, T.-Y. Luo, C.-C. Hwang, and B.-Y. Chang, "Field path design assessments of a high-performance small-power synchronous-reluctance motor," *IEEE Trans. Magn.*, vol. 51, no. 11, 2015.
- [19] A. Vagati, G. Franceschini, I. Marongiu, and G. Troglia, "Design criteria of high performance synchronous reluctance motors," in *Industry Applications Society Annual Meeting, 1992., Conference Record of the 1992 IEEE*. IEEE, pp. 66–73, 1992.
- [20] A. Vagati, A. Canova, M. Chiampi, M. Pastorelli, and M. Repetto, "Improvement of synchronous reluctance motor design through finite element analysis," in *Industry Applications Conference, 1999. Thirty-Fourth IAS Annual Meeting. Conference Record of the 1999 IEEE*, vol. 2. IEEE, pp. 862–871, 1999.



Tefera Kitaba Tolesa received the B.Tech degree in electrical power engineering from the Defence Engineering University, Bishoftu, Ethiopia, and the M.E. degree in power electronics and Drives from Anna University, Chennai, India, in 2007 and 2012, respectively. He is currently working toward the Ph.D. degree from Indian Institute of Technology

Guwahati, India. His current research interests include the design and modelling of electrical machines, renewable Energy, and power electronics.



Praveen Tripathy (M11) received the Ph.D. degree in electrical engineering from the Indian Institute of Technology Kanpur, India, in 2011. He is currently an Associate Professor with the Department of Electronics and Electrical Engineering, Indian Institute

of Technology Guwahati, India. His research interests include wide area monitoring and control, power system dynamics, power system operation and control, FACTS, distribution automation, and wind energy systems.



Ravindranath Adda (S11) received the Ph.D. degree in electrical engineering from the Indian Institute of Technology Kanpur, India, in 2014. He is currently an Assistant Professor with the Department of Electronics and Electrical Engineering, Indian Institute of Technology Guwahati,

India. His research interests include Power Electronics, Distributed Generation and Power Quality.